REPORT DOCUMENTATION PAGE

AFRL-SR-BL-TR-02-

0082

1. REPORT DATE (DD-MM-YYYY)	2. REPORT TYPE	Dec.1,1997-May 31, 2001
02/20/2002	Technical - Final	

4. TITLE AND SUBTITLE
Barrier to aggregation for light-atom dopants of Solid hydrogen

5a. CONTRACT NUMBER
F49620-98-1-00-45

5b. GRANT NUMBER
F49620-98-1-00-45

5c. PROGRAM ELEMENT NUMBER
61102F

5d. PROJECT NUMBER
2303

5e. TASK NUMBER
EX

5f. WORK UNIT NUMBER

6. AUTHOR(S)
G. Scoles and K. K. Lehmann

7. PERFORMING ORGANIZATION NAME(S) AND ADDRESS(ES)
Princeton University, Department of Chemistry, Princeton, N.J.08544

8. PERFORMING ORGANIZATION REPORT NUMBER

9. SPONSORING / MONITORING AGENCY NAME(S) AND ADDRESS(ES)
AFOSR/NL
801 North Randolph Street
Room 732
Arlington, VA 22203-1977

10. SPONSOR/MONITOR'S ACRONYM(S)

11. SPONSOR/MONITOR'S REPORT NUMBER(S)

12. DISTRIBUTION / AVAILABILITY STATEMENT
distribution unlimited

13. SUPPLEMENTARY NOTES
helium, hydrogen, clusters, chemical metastability, spectroscopy

14. ABSTRACT

In this report the development of the use of spectroscopy in highly quantum clusters made of H_2 or He to study the possibility to increase the energy contents of solid H_2 by seeding in it, in a stable way, relatively high (~5%) of light metal atoms or complexes. Experimental results on the solvation (or lack of it) of metal atoms (Mg and Al) with both spherical (Mg) and not-spherical (Al) outer electronic shells are discussed and compared with theoretical predictions. Theoretical results on the improvement of models to calculate intermolecular potentials in hard atom-soft atom interactions are also discussed. Finally, the progress towards assembling a facility for Stimulated Raman Scattering measurements in molecular beams of doped and undoped H_2 cluster is reported. The latter facility should enable the determination of several parameters for metal-doped condensed H_2 which are essential to the determination of the viability of doped H_2 as a rocket fuel.

15. SUBJECT TERMS

20020322 054

16. SECURITY CLASSIFICATION OF:			17. LIMITATION OF ABSTRACT	18. NUMBER OF PAGES	19a. NAME OF RESPONSIBLE PERSON
a. REPORT	b. ABSTRACT	c. THIS PAGE			G. Scoles
unclass	unclass	unclass		24	19b. TELEPHONE NUMBER (include area code) (609) 258-5570

BARRIER TO AGGREGATION FOR LIGHT-ATOM DOPANTS OF SOLID HYDROGEN

G. Scoles and K. K. Lehmann
Chemistry Department
Princeton University
Princeton, N. J. 08544

Final technical report on the Grant F49620-98-0045

Prepared for the Air Force Office of Scientific Research

Table of contents

Supported Personnel and Collaborators

a) Personnel: J. Higgins (Princeton, graduate student)
U. Merker, (A. von Humboldt Foundation Post-Doctoral Fellow)
M. Radcliff (Princeton, graduate student)
J. Reho (Princeton, graduate student)
I. Scheele, (Visiting student from Bochum University, Germany)

b) Collaborators: K. K. Lehmann (Chemistry Department, Princeton) (Co-PI)
M. Gutowski (Pacific Northwest National Lab)
T. S. Ho (Senior Chemist, Princeton University)
T. Hollebeek (Princeton, graduate student)
G. Murdachaew (U. of Delaware, graduate student)
S. Nayak (Princeton, Research Fellow)
M. Nooijen (Chemistry Department, Princeton)
H. Rabitz (Chemistry Department, Princeton)
A. Ray (University of Texas at Arlington)
J. Sin (Princeton, graduate student)
K. Szalewicz (Physics Department, U. of Delaware)

1.0 Objectives and their evolution

Light atom doped solid hydrogen is one of the most promising candidates for a practical HEDM that can be used to improve the performance of both civilian and military launch vehicles. An important goal of research in this field is to determine the maximum concentrations that can be achieved while maintaining a high energy density of the fuel. Answering this question requires improved understanding of hydrogen-dopant and dopant-dopant interactions and the mobility of dopants in both liquid and solid hydrogen. Our contribution to this effort has been the development and exploitation of methods to produce and spectroscopically characterize metal doped quantum clusters made of hydrogen and/or helium. Our work complements ongoing research on doped solid hydrogen at Edwards AFB.

Using spectroscopy as a diagnostic tool our program aimed at the study of metal-doped H_2 clusters in order to investigate the possibility that certain light atoms or their dimers may have small, but significant, barriers to the formation of covalently bound larger clusters. At the temperature of solid hydrogen fuels, the presence of even small activation barriers (on the order of 0.2 kcal/mole) will reduce the rate of chemical bond formation. As the rate of bond formation becomes lower, higher dopant concentrations could be realized in condensed hydrogen fuel.

The first approach we have explored is to exploit small barriers that may arise in the recombination of some atoms due to the need to decouple spin-orbit interactions in order to have atomic orbitals that can participate in bonding. This approach arose from our previous work on the dynamics of excited states of alkali atoms on the surface of helium nanodroplets, where such barriers were shown to strongly influence the dynamics. A second approach is to build up van der Waals clusters of alkaline earth atoms, such as Be or Mg, which are closed shell species and thus may have small barriers to 'metallization.' By thus keeping the size of the cluster below the metallization limit, the energy contents of the fuel is optimized. A third approach is to saturate the interactions, thus kinetically preventing the formation of covalent bonds.

A recent theoretical investigation of boron-doped H_2 matrices by Voth, Alexander and collaborators has shown that at a concentration of a few percent a boron-doped H_2 matrix should be stable. On the other hand experimental work by Fajardo and collaborators at the AFRL (Edwards AFB) has failed to show that in the case of Al doping such concentration can be reached as catastrophic atom-atom recombination seems to set in already at concentrations below the 1% level. However, it is quite likely that the diffusional processes that lead to the unstablization of the matrix occur at the moment the matrix is formed. This is because the high H_2 flux needed to obtain transparent matrices (i.e., matrices that can be probed) leads necessarily to "warm" surface conditions which, in turn, allow for dopant diffusion. (The latter is also favored by the fact that, at present, the Al atom flux comes from a hot metal source).

The study of metal-doped H_2 clusters (with or without a liquid He coating) in progress in our laboratory aims a better understanding of the location of the dopant in the cluster towards an evaluation of the feasibility to produce higher (~5%) metal-doped matrices by cluster deposition instead of beam (gas) deposition as used at present at the AFR Laboratory.

Since the results obtained in the early part of the reporting period, on the visible/uv spectroscopy of Mg and Al atom-doped He clusters had shown the limits of this type of diagnostic (too broad lines instead of strong inelastic probe atom/matrix interactions) we have concentrated in the second half of the period on obtaining IR spectra of molecule doped H_2 clusters and on interpreting the results obtained last year. We have made strong progress on the interpretation side so that a.) we can now predict with confidence the

location of a guest atom in a quantum cluster made of He or H_2 and b.) we understand both the multiplicity and the lifetimes of the spectra measured last year. We have instead failed in obtaining IR spectra of molecules embedded in H_2 clusters. This is likely due to the fact that we are limited by the 5000-6700 cm^{-1} frequency range of our tunable laser system which gives us easy access to the overtone region of CH chromophores. It is likely that these overtone excitations relax too rapidly in H_2 clusters producing spectral features too broad to be detected within our ultrahigh-resolution apparatus.

Two years ago we have been fortunate to obtain a DURIP grant with which we have purchased a new laser system (an Indigo laser manufactured by Positive Light) which, in combination with a laser built in our laboratory, was designed to obtain high resolution Raman spectra of both metal-doped and undoped clusters. Unfortunately when the Indigo laser arrived about 14 months ago it did not meet our expectations with respect to linewidth and stability. On the other hand, as it was satisfactory with respect to the repetition rate and the average power levels that it could reach, and because there was not an alternative solution available on the market, we decided to tough it out and fix the laser ourselves. This effort, which resulted to be somewhat more difficult than expected, lasted approximately one year; but now (see also the DURIP grant # F49620-00-1-0192 final report filed at the same time as the present one) we are happy to report that the laser delivers an average power of 1.5 Watts at the repetition rate of 1 kHz with pulse length 10 ns and bandwidth of 725-830 nm. This level of performance, which makes our system a rather unique piece of equipment, should, barring unforeseen circumstances, allow us in the next few months to obtain Raman spectra of both doped and undoped hydrogen cluster beams. Raman excitation of H_2 molecules should show much narrower spectral features which, by shifts and splittings, should also reveal the presence and location of eventual metal atom dopants. In this way the problems described above should be eliminated and a rich selection of experimental possibilities should become available.

2. Accomplishments/New findings

Contents:

2.1 Time-resolved studies of complexes involving alkali atoms

2.1.1 Dynamics of alkali-helium excimers

The formation of a Na*-He excimer upon optical excitation of a Na atom on the surface of a helium droplet has been previously demonstrated in our laboratory.[1,2] The emission is red-shifted from the Na atomic lines and can be quantitatively modeled from the potential curves of J. Pascale.[3] Using time-correlated single photon counting we have measured the onset of fluorescence from the Na*-He excimer; depending on which Na excited state we access, we see different rates of fluorescence. The rise time of excimer fluorescence after excitation of the Na $3P_{1/2}$ line was found to be 700 ps, while after exciting the Na $3P_{3/2}$ line the rise time was found to be 70 ps.

The difference in rise time has been attributed to spin-orbit mixing of the $^2\Pi_{1/2}$ surface of NaHe with the $^2\Sigma$ surface, generating a small (0.7 cm^{-1}) barrier on the $^2\Pi_{1/2}$ (which asymptotically corresponds to the

		Na_2 B-X	Na atom P-S	Na_2 B-X	Na atom P-S
v	j	RiseTime (±20ps)	RiseTime (±20ps)	FallTime (±0.1ns)	FallTime (±0.1ns)
4	5/2	222	345	6.65	16.26
3	5/2	385	434	6.64	16.28
3	1/2	370	417	6.67	16.29
2	5/2	427	445	6.68	16.24
2	1/2	382	438	6.65	16.28
1	1/2	890/990	770/1110	6.65	16.26
0	0	1550/1300	770/2100	6.65	16.28

Table 1. Rise and fall times of intersystem crossing products due to quartet Na trimer excitation. The columns v and j indicate the quantum numbers of the excited trimer bands (listed in order of descending energy).

Na J=1/2 level) but no barrier on the $^2\Pi_{3/2}$ curve (asymptotically, the J=3/2 level). Even though this barrier is small, there will be significant effects on the dynamics due to the extremely cold He droplet environment. A similar spin-orbit induced barrier as been observed for Ag*-He (in bulk liquid helium).[4]

We have also characterized the formation of the K*-He excimer formed after optical excitation of K atoms on the surface of a He droplet. Again, the dispersed emission is red-shifted and can be modeled using the KHe surfaces of Pascale.[3] The fit is good except in the red tail which may be due to excessive stiffness in the upper state repulsive wall, or to possible higher-order K*-He_n exciplexes.

In order to compare to Na*-He, we have measured the onset of the red-shifted emission from excitation of K atoms. We record a rise time of the excimer fluorescence of 200 ps, quite smaller than for the comparable Na*-He case. One would expect an increase in the size of the barrier on the $^2\Pi_{1/2}$ surface (because of the larger spin-orbit splitting), leading to a longer time before onset of fluorescence. However, the spin-orbit splitting is not the only factor. One must also consider the long range dispersion interaction to properly predict the presence and magnitude of a barrier along the spin-orbit decoupled potential energy surface.

v	j	Fall Time (±0.1 ns)
4	5/2	523/745
3	5/2	533/738
3	1/2	535/735
2	5/2	529/741
2	1/2	668/952
1	1/2	1020
0	0	1160

Table 2. The lifetimes of the v, j vibrational levels of the $2^4E'$ state of Na_3.

In the case of KHe, the dispersive forces are much stronger than for NaHe. For KHe, the C_6 coefficient is 38.9 atomic units, but only 25.5 a.u. for NaHe[5]. Any potential barrier that is formed through spin-orbit interaction is tempered by the relative strength of the long range attractive forces, resulting in a reduced barrier and faster onset of excimer fluorescence. Two papers have been published on this subject in the Journal of Chemical Physics[6,7].

2.1.2 Dynamics of alkali quartet trimers

We have examined the curve crossing undergone by spin-polarized Na_3 upon optical excitation to various vibronic bands of the $2^4E'$ electronic state.[8,9] The excited quartet state crosses to a predissociative doublet state, opening two emission channels from the doublet trimer: dissociation into a singlet dimer and an excited atom, or an excited dimer and a ground-state atom. In both channels, fluorescence is blue-shifted from the excitation frequency. K_3 goes through a similar spin-flip reaction when electronically excited in the quartet manifold.

For both species, we have measured the intersystem crossing times as a function of excited quartet vibronic band. The crossing time is obtained by timing the onset of fluorescence, using filters to select the desired channel. The rise times, after excitation of different vibronic bands, for both the Na_2 singlet ($B \rightarrow X$) and Na atomic ($3P \rightarrow 3S$) emission are listed in Table 1, along with the

measured lifetimes of the (B) $1^1\Pi_u$ state and the atomic 3P state. The lifetimes of both states correspond well with the gas-phase literature values,[10] indicating the products of the spin-flip are no longer attached to the droplet surface.

The onset time represents the time needed to populate the two emission channels, which is also the time needed for intersystem crossing from the quartet to the doublet manifold. Since the branching ratio between the two channels is constant with respect to the quartet vibronic band excited, we can conclude that there is a single access window into the doublet manifold, located near 16030 cm^{-1}. A paper has been published in the Journal of Chemical Physics on this subject[11].

The resonant fluorescence of quartet Na_3 has also been measured in time. This is the excitation to the $2^4E'$ state, which then fluoresces back to the ground quartet state, $1^4A_2'$. All the rise times are under 40 ps, which is the limit of our instrument, while the fall times are several hundred nanoseconds (see Table 2) and biexponential. As excitation energy is increased, the decay time of the resonant fluorescence decreases. This matches the trend of the rise time of both the atomic and dimer fluorescence. Further, that the lifetimes of the excited quartet states closely match the onset time of the products provides evidence for the minimal influence of the helium droplet, since the majority of depopulation occurs through intersystem crossing and radiative decay. From the resonant fluorescence spectra we have obtained substantial information on three-body forces in low Ionization Potential atoms and published a paper on this subject in the Journal of Chemical Physics[12].

2.1.3 Dynamics of triplet potassium dimers

Along with curve-crossing in alkali trimers, we have also observed in the $1^3\Pi_g \leftarrow 1^3\Sigma_u^+$ transition of K_2 not only atomic 4P→4S emission but also K_2 $B(^1\Pi_u) \rightarrow$ and $A(^1\Sigma_u^+) \rightarrow X(^1\Sigma_g^+)$ dimer emission. This emission is again blue-shifted and indicative of an intersystem crossing mediated by the environment of the helium droplet. While scanning over the $1^3\Pi_g \leftarrow 1^3\Sigma_u^+$ transition, we selectively collected the B→X and A→X singlet emissions. The fluorescence from molecular emission is shifted 83 cm^{-1} to the red of the fluorescence from atomic emission after the same excitation.

Time-resolved studies were made of the fluorescence arising from the $1^3\Pi_g \leftarrow 1^3\Sigma_u^+$ excitation, particularly the rise times of the emission from all three species produced. For both singlet states, the fluorescence starts 65 ps after excitation, while the atomic fluorescence occurs in less than 50 ps.

The potential surface of the $1^3\Pi_g$ state of K_2 contains four vibrational levels held behind a small barrier. There is an 83 cm^{-1} separation between the first and fourth levels. The lifetime of these levels decreases as the vibrational number increases. We can conclude that excitation into the higher vibrational levels of the triplet excited state causes dissociation and atomic fluorescence. And excitation into the lower vibrational levels (primarily v'=0, the only level with a lifetime > 60 ps) will lead to an intersystem crossing and singlet dimer fluorescence. On this subject we have published a paper in the Discussions of the Faraday Society[13].

2.2 Solvation of Mg atoms in superfluid helium droplets

2.2.1 Mg atom excitation spectra

Our measurement of the $3^1P_1^0 \leftarrow 3^1S_0$ transition of Mg atoms in helium nanodroplets shows evidence that this atom is solvated in the interior of the droplets (see Figure 1). The absorption is broadened by the droplet (FWHM of 660 cm^{-1}) and blue-shifted from its gas-phase transition ($\Delta\nu$ = 307 cm^{-1} and 642 cm^{-1}). The spectrum shows a splitting into two components that are attributable to quadrupolar deformations of the helium cavity

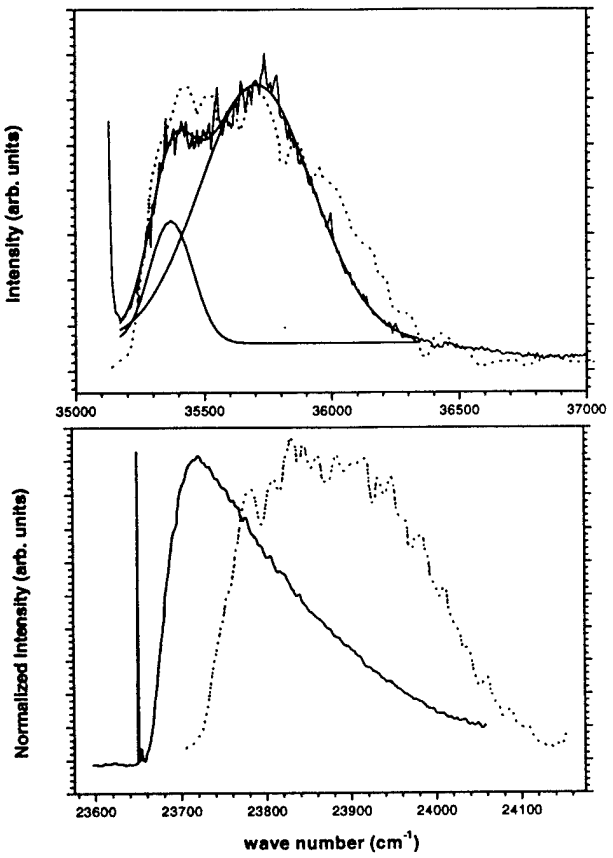

Figure 1. (upper panel) The $3^1P_1^0 \leftarrow 3^1S_0$ transition of Mg atoms solvated in helium nanodroplets. The best fit to the data by two Gaussian lineshapes is also shown (solid lines). Also, the same transition in bulk liquid helium (dots). **(lower panel)** The same transition in Ca; both in helium nanodroplets (solid), and in bulk liquid helium (dots).

surrounding the atom. This splitting has been seen by Kinoshita *et al.*[14] in D_2 ($n^2 P_{3/2} \leftarrow n^2 S_{1/2}$) excitation of Cs ($n = 6$) and Rb ($n = 5$) atoms in bulk liquid helium, as well as our studies of Al[15] atoms solvated in liquid helium droplets.

As the droplet spectrum matches the spectra taken in a bulk liquid helium matrix[16], the similarity of the two spectra speaks in favor of solvation. In contrast, alkali atoms (on the helium droplet surface) exhibit only small shifts from their gas-phase frequencies. By comparing Ca on a droplet[17] with Ca in bulk liquid helium[18], we can see that it holds an intermediate position between solvated and surface locations, having only one-half of the broadening and one-third of the shift as the bulk helium spectra.

2.2.2 Mg atom time-resolved measurements

Along with the excitation spectra, we have temporally dispersed the fluorescence emitted after $3^1P_1^0 \leftarrow 3^1S_0$ excitation of the solvated Mg atoms (see Figure 2). Both the gas-phase and the droplet-solvated Mg spectra are well fit by a model employing a single exponential rise and a single exponential fall. The fall time (*i.e.*, lifetime) of 2.05 ± 0.05 ns found for the $3^1P_1^0$ state emission of gas-phase Mg agrees well with the literature value (1.99 ± 0.08 ns)[19], while the rise time fit to the data is instrument-limited (i.e., < 50 ps). For solvated Mg atoms in the droplet, the lifetime is found to be 2.39 ± 0.05 ns, which is 20% longer than the gas-phase value.

The lengthening of the lifetime for the solvated atom can be ascribed to two sources, the first being the red-shift of the emission frequency. Since the rate of spontaneous emission scales with the cube of the frequency, a lower emission frequency will give a longer lifetime. Assuming a red-shift similar to that of Mg atoms solvated in bulk liquid helium[16], which is 3.2 ± 0.2 nm, accounts for a 3.5% increase in the emission lifetime.

The second cause of the increased lifetime is the helium solvent itself. The dielectric response of the solvent will result in an induced transition dipole that will interfere with the transition dipole of the chromophore. By summing over all the dipoles induced by the radiating dipole, we can write the net induced dipole as the following integral:

$$\mu_{IND} = \mu \cdot 2\alpha \cdot \int \rho(\vec{r}) \cdot P_2(\cos\theta) \cdot r^{-3} dv$$

where r is the distance, α is the polarizability volume of He (0.206 Å^3), and θ is the angle between the chromophore transition dipole and the displacement to a generic point in the He cluster. Taking into account the anisotropic He density around the excited Mg atom, shown in Figure 3, (with high density at the node of the

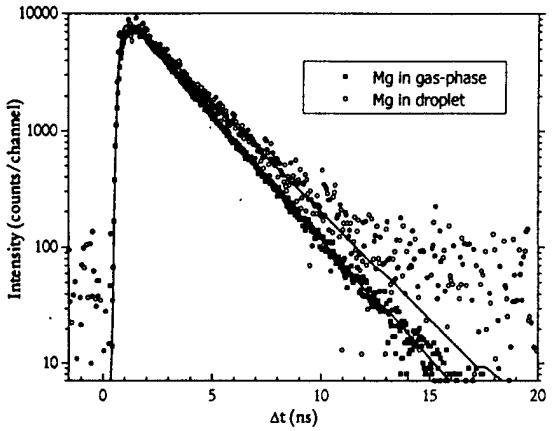

Figure 2. Log plot of the time evolution of gas-phase (filled squares) and droplet-solvated (open circles) Mg atoms upon $3^1P_1^0 \leftarrow 3^1S_0$ excitation. The droplet-solvated data are normalized to the gas-phase data for visual comparison. The solid lines are the best fits to the data.

p orbital, which is parallel to the transition moment), the induced moment is 6.2% of the bare Mg transition moment. This leads to a predicted lifetime lengthening of 14%. When combined with the 3.5% from the emission frequency, we predict a lifetime 17.5% longer than the gas-phase value. Our experimental value of $20 \pm 3\%$ adds further evidence of solvation by the helium droplet. These results have been published in ref. 20.

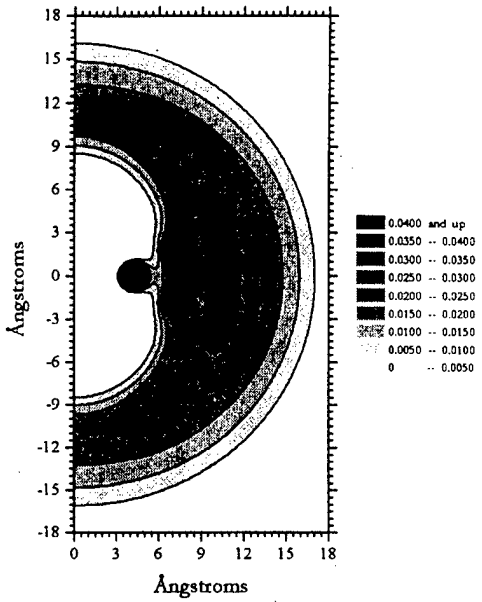

Figure 3. He density contour plot calculated via Density Functional Theory in which a ground state Mg atom is constrained to be in the center (*i.e.*, at 0, 0) of a 300-atom helium droplet.

	$\varepsilon(K)$	$r_{min}(Å)$	λ	$IP(eV)$
Cs	1.2	7.7	0.66	3.9
Rb	1.4	7.3	0.73	4.2
K	1.0	7.7	0.59	4.3
Na	1.7	6.5	0.85	5.1
Li	2.2	6.1	1.01	5.4
Ca	3.7	6.4	1.8	6.1
Mg	5.6	5.3	2.2	7.6

Table 3. λ values from HFD dopant-He potentials. Threshold of solvation should be between Ca and Mg.

3.3 Mg-He potential energy surfaces

Ancilotto *et al.*[21] have used the dopant-He pair potential to devise a relatively simple model that treats the question of solvation. They propose that solvation can be predicted by means of a dimensionless parameter λ which compares the gain in energy due to the dopant-helium interaction against the energetic cost of creating a cavity within the liquid. Formally,

$$\lambda \equiv \rho \varepsilon r_{\min} \sigma^{-1} 2^{-1/6}$$

where ρ is the helium density, σ is the surface tension of the liquid, and ε and r_{min} are the well depth and equilibrium bond distance of the dopant-He pair potential, respectively.

Using helium density functional calculations, Ancilotto *et al.*[21] predict that atoms with values of $\lambda < 1.9$ reside on the surface, while dopants with $\lambda > 1.9$ remain solvated. The model successfully predicts exterior locations for alkali atoms ($\lambda \cong 0.7$) and interior locations for Ag ($\lambda \cong 5$) and SF_6 ($\lambda \cong 19$). Table 3 lists the parameters for several alkali and alkaline earth solvated atoms.

We have evaluated the potential energy surfaces of systems at the border region of the Ancilotto model. In so doing, we have produced the $(X)1^2\Sigma$ surfaces of MgHe and CaHe using the Hartree-Fock Damped Dispersion ansatz, a widely used semi-

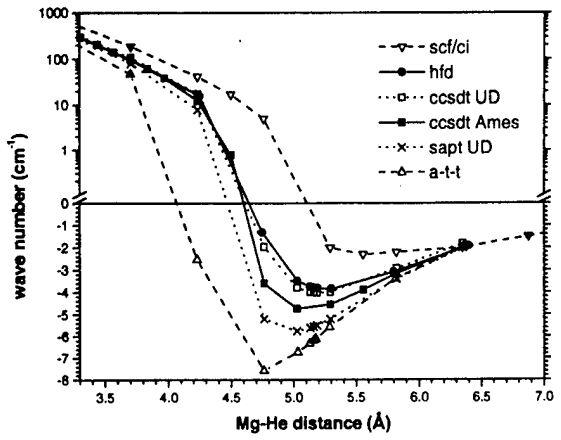

Figure 4. Potential surfaces of MgHe.

empirical method which has been found to be quite accurate for atom combinations involving atoms of the first and second rows of the periodic table[22,23].

Figure 4 illustrates the MgHe $(X)1^2\Sigma$ state as calculated by several methods. Well depth ε and equilibrium internuclear distance r_{min} for these surfaces are reported in Table 4. Of the surfaces available for both dopants only the HFD and CCSD(T) yield λ values for Mg and Ca that follow the expected trend. The CCSD(T)/Ames MgHe potential gives a λ value of 2.6, correctly predicting solvation; for Ca, a λ value of 2.2. This is just over the threshold for solvation predicted by the Ancilotto model, establishing the "borderline" nature of Ca attached to liquid helium droplets. One way to picture the "borderline" case is a half-submerged atom with ripples of helium density passing over the top.

Helium density functional studies have been used as well to explore this situation. Our density functional studies were done using code for helium with impurity atoms in which the dopant atom is treated as a classical object (*i.e.*, devoid of zero point energy) in a quantum liquid[28,29]. Previous calculations employing these programs have been found to be in good agreement with Monte Carlo simulations[30].

In these studies, the solvation energy $E_{solvated}$ of the guest atom inside a He_n droplet

	$\varepsilon(cm^{-1})$		$r_{min}(Å)$		λ	
	Mg	Ca	Mg	Ca	Mg	Ca
SCF/CI	2.3	2.9	5.6	7.4	1.4	2.1
A-T-T	7.7	10.3	4.7	5.1	3.8	5.5
HFD	3.9	2.6	5.3	6.4	2.22	1.82
CCSD(T)/Ames	4.8	3.3	5.1	6.0	2.65	2.16
CCSD(T)/UD	4.0		5.2		2.2	
SAPT	5.8		5.0		2.7	

Table 4. Comparison of the well depth (ε), internuclear distance (r_{min}), and the λ paramter of Ancilotto *et al.*[21] for the $1^2\Sigma$ surfaces of MgHe and CaHe as calculated by the SCF/CI[24], A-T-T[25], HFD[20], CCSD(T)/UD[26], SAPT[26], CCSD(T)/Ames[27] methods.

Dopant	$E_{surface}(K)$	$E_{solvated}(K)$
Na	-11	+46
Ca	-7.5	+80
Mg-HFD	-21	-0.2
Mg-CCSD(T)/UD	-16	+2.7
Mg-SAPT	-32	-41

Table 5. Energies from density functional calculations for various dopants in and on a helium droplet of 300 helium atoms. All energies are normalized to the droplet-dopant asymptote.

(n = 300) is compared with the energy of the same atom resident on the surface of a droplet of the same size. The dopant atom is treated as an external potential around which the helium density is allowed to adjust based upon minimization of the total energy of the system. $E_{surface}$ is calculated with the dopant fixed at 16 Å from the center, corresponding to the radius of the 300-atom droplet, while $E_{solvated}$ has the dopant constrained to be at the center of the droplet.

The DFT results for Na and Ca, in Table 5, are correctly predicted to be unstable when solvated, but the Mg results are unfortunately not right. All three MgHe potentials lead to minima when on the surface; only the SAPT potential (which is too deep) also has a minimum in the interior. This is more a function of the density functional putting too much emphasis on the repulsive wall than of the SAPT potential being correct. Looking at the He density profiles, it is clear that the SAPT potential creates a smaller cavity in the helium and is therefore less likely to be expelled to the surface (see fig. 5).

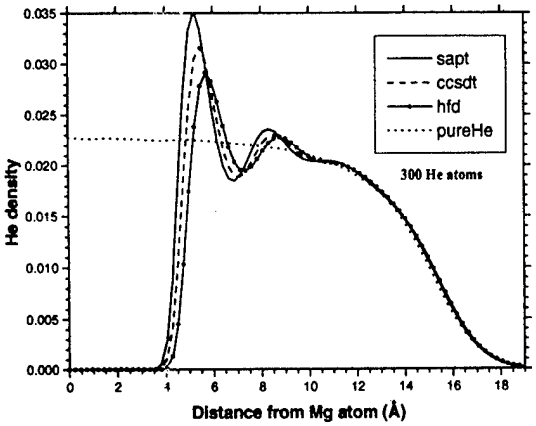

Figure 5. Profiles of helium density from three different pair potentials surrounding a dopant at center of 300 atom nanodroplet. The density for a droplet without a dopant is also shown.

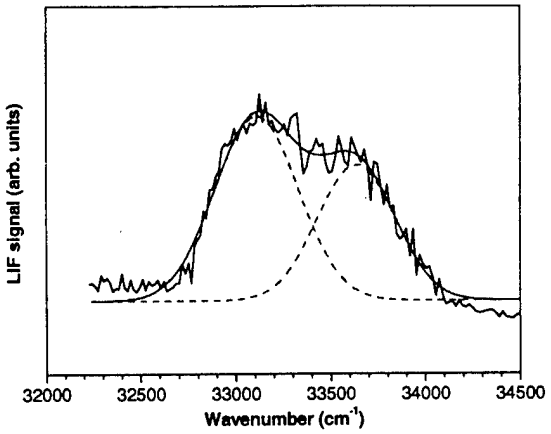

Figure 6. The $3^2D \leftarrow 3^2P$ transitions of Al atoms solvated in helium nanodroplets. The fit to the spectrum (solid line) is a summation of two Gaussian lineshapes (dotted lines).

2.3 Solvation of Al atoms in superfluid helium droplets

2.3.1 Al atom excitation spectra

We have measured the LIF spectrum of the $3^2D \leftarrow 3^2P$ transition of Al atoms in superfluid helium nanodroplets (see Figure 6). The spectrum shows the Al atoms are located inside the liquid droplet, having a large blueshift (roughly 1000 cm^{-1} from the gas-phase transition) and being quite broadened (fit to two gaussians with FWHM > 400 cm^{-1}, separated by > 500 cm^{-1}). The observed splitting is much larger than the gas-phase $3^2P_{3/2} - 3^2P_{1/2}$ level separation; we have performed calculations which indicate that the orbital angular momentum in the 3^2P state is quenched by the helium matrix due to the strongly anisotropic interactions with the helium.

2.3.2 Al atom time-resolved measurements

Lifetime measurements of excited Al atoms (see fig. 7) were accomplished using our time-correlated single photon counting apparatus. Temporal evolution of the total fluorescence from excitation of the $3^2D \leftarrow 3^2P$ transition yielded lifetimes of 6.4 ± 0.1 ns, in marked disagreement with the known lifetimes of the $3^2D_{5/2}$ and $3^2D_{3/2}$ states (13.5 ns and 13.3 ns, respectively)[31].

Using a band-pass filter to select only the $3^2D \rightarrow 3^2P$ emission resulted in no fluorescence being collected, whereas a filter passing only fluorescence from the $4^2S \rightarrow 3^2P$ transition yielded data with the same 6.4 ns lifetime. Exciting directly to the 4^2S state also gives a 6.4 ns lifetime. It is apparent that the initially-populated $3^2D_{5/2,3/2}$ states of Al are quenched to the 4^2S state on a sub-nanosecond time scale due to interaction with the He matrix. This entails a transfer of nearly 7100 cm^{-1} of energy into the surrounding helium. This energy corresponds to the evaporation of over 1400 helium atoms from the cluster in order to re-establish the pre-quenching cluster temperature of 0.37 K, assuming that all 7100 cm^{-1} of energy goes into evaporation. These data have been published in ref. 15.

2.3.3 Al-He potential energy surfaces

The $(X)1^2\Pi$ and $1^2\Sigma$ potential energy surfaces of AlHe have been calculated using the Hartree-Fock Damped Dispersion (HFD) ansatz[22]. The ΔE_{SCF} component was calculated in the 6-311++G** basis using the Gaussian 98[32] program suite, correcting at each point for

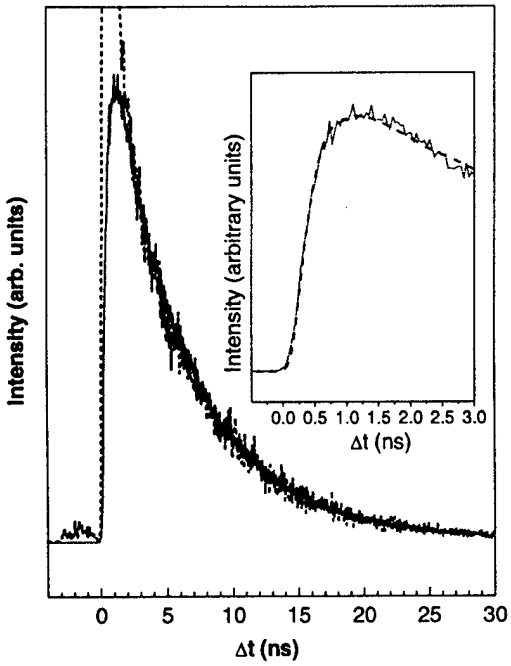

Figure 7. Dotted line: Temporally dispersed fluorescence of Al atoms upon excitations near the $3^2D \rightarrow 3^2P$ transition of Al. The rising edge is masked by scattered light. Solid line: Temporally dispersed fluorescence of Al atoms upon excitations near the $3^2D \rightarrow 3^2P$ transition of Al, detecting only frequencies near the $4^2S \rightarrow 3^2P$ transition frequency region of Al. The inset highlights the rising edge (solid curve) and the best fit to the data (dotted curve).

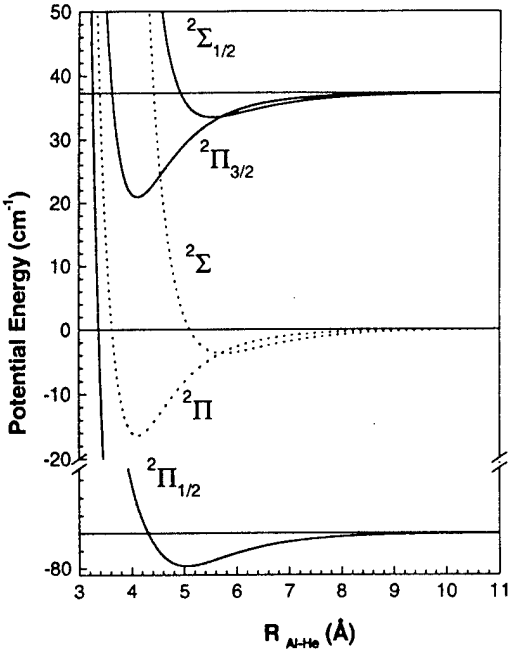

Figure 8. Spin--orbit averaged $1^2\Pi$ and $1^2\Sigma$ and spin--orbit-decoupled $1^2\Sigma_{1/2}$, $1^2\Pi_{1/2}$, and $1^2\Pi_{3/2}$ potential energy surfaces of AlHe.

parameter	*$1^2\Sigma$ Al-He*	*$1^2\Pi$ Al-He*
C_6	1.6695×10^5	8.6183×10^4
C_8	2.1140×10^6	1.0913×10^6
C_{10}	3.7354×10^7	1.9283×10^7

Table 6. C_n coefficients used in generating the $1^2\Pi$ and $1^2\Sigma$ Al-He HFD surfaces. All energies in cm^{-1} and distances in Å.

basis set superposition error. The correlated (ΔE_{corr}) component makes use of the AlHe long range coefficients C_n calculated using the AlAr C_n coefficients of LePicard *et al.*[33], the Ar_2 and He_2 C_n coefficients of Standard and Certain[34], and standard combination methods[35]. These C_n coefficients used in generating the $1^2\Pi$ and $1^2\Sigma$ AlHe HFD surfaces are listed in Table 6.

Spin-orbit coupling of the $1^2\Pi$ and $1^2\Sigma$ AlHe HFD surfaces yields the solid curves given in Figure 8, again with energies referred to the original Al([Ne]$3s^23p^1$) + He($1s^2$) asymptote.

When spin-orbit interaction is included, the $1^2\Pi$ surface is found to split into a $1^2\Pi_{1/2}$ and $1^2\Pi_{3/2}$ surface, the former of which mixes with the $1^2\Sigma_{1/2}$ state and thus has a minimum of potential at larger internuclear distance (5.05 Å) than either the $1^2\Pi_{3/2}$ or the spin-orbit averaged $1^2\Pi$ surface. Characteristic parameters of these surfaces are given in Table 7. The $1^2\Pi$ surface is seen to have a minimum at 4.12 Å while the $1^2\Sigma$ minimum occurs at an AlHe distance of 5.77 Å.

After generation of our HFD AlHe surfaces, we have used them to investigate the nature of Al electron localization for the Al-He_n system. In particular, the main question addressed here is whether the ground state Al valence is best described by the spin-orbit decoupled $1^2\Pi_{3/2,1/2}$ surfaces or by the spin-orbit averaged $1^2\Pi$ surface (aspherical). In the former case, we expect only the lower-energy

	R_{min}(Å)	$\varepsilon(cm^{-1})$	$\sigma(cm^{-1})$
$1^2\Pi$	4.12	16.45	3.64
$1^2\Sigma$	5.77	3.74	5.1
$1^2\Pi_{3/2}$	4.12	16.42	3.64
$1^2\Pi_{1/2}$	5.05	4.97	4.32
$1^2\Sigma_{1/2}$	5.54	3.81	4.94

Table 7. Parameters of the AlHe potenetial energy surfaces as calculated by the HFD ansatz.

($1^2\Pi_{1/2}$) surface to be populated due to the cold environment of the helium droplet. The Al electron density correlating with this state is spherical. If the spin-orbit interaction is quenched in the helium, however, the spin-orbit averaged $1^2\Pi$ surface, with an aspheric Al electron density, would describe the Al-He_n interaction. The upper frame *a* of Figure 9 compares the $AlHe_n$ (n = 1, 4, 6, 7, 8) $1^2\Pi$ potential energy surfaces based upon our $1^2\Pi_{1/2}$ AlHe HFD results used under the assumption of additivity.

These surfaces are created by arranging the helium atoms in symmetric polygons in the nodal plane around the *p* orbital of Al. From the figure it is seen that a minimum appears at distances which are near the initial spin-orbit averaged $1^2\Pi$ minimum (4.13 Å), while the $1^2\Pi_{1/2}$ minimum at 5.05 Å goes through a "shelf" state and almost disappears. We can thus conclude that as the number of He atoms around the node of the Al atom increases the mixing of Σ character into the $1^2\Pi$ state, predicted by spin-orbit mixing, becomes less and less. This lack of Σ character corresponds to less Al valence electron density in the *xy* plane (*i.e.*, the plane defined by the He_n polygons), creating an attractive region into which the He atoms can be drawn. Another way to view these changes in the potential energy surfaces is as representative of the localization of the Al valence electron in its p_z orbital (*i.e.*, the Al *p* orbital perpendicular to the plane defined by the He atoms), which occurs to a greater extent as n increases. Thus these additive surfaces support the conclusion that the spin-orbit decoupling is quenched in the helium solvent so that the density profile of

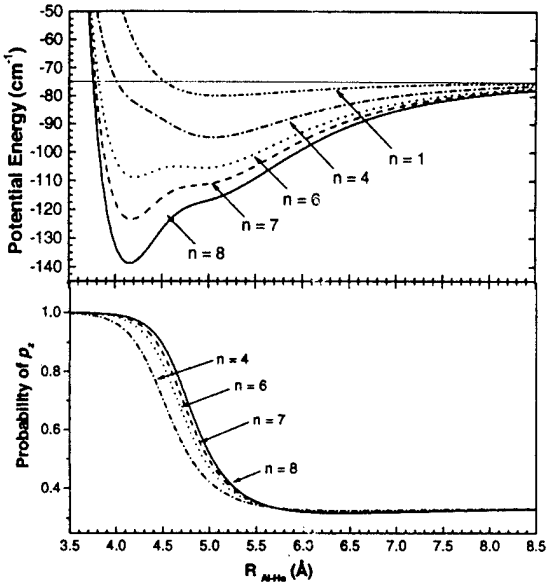

Figure 9. (upper panel) $1^2\Pi$ potential energy surfaces of AlHe (dot-dot-dash line), $AlHe_4$ (dot-dash line), $AlHe_6$ (dotted line), $AlHe_7$ (dashed line), and $AlHe_8$ (solid line), where the helium atoms are arranged symmetrically on the xy plane around the Al p_z orbital. **(lower panel)** Probability of occupation of the Al p_z orbital as a function of the Al-He distance for each of the $AlHe_n$ configurations depicted above, using the same line designations.

the Al *p* electron takes on the aspherical p_z character.

The lower frame *b* of Figure 9 shows the probability of occupation of the p_z orbital as a function of Al-He distance for the $AlHe_n$ (n = 4, 6, 7, 8) surfaces depicted in the upper frame of the Figure. The distance coordinate corresponds to a symmetric "breathing" of the polygonal He ring. It is found in comparing the two frames that the movement from spin-orbit averaged (0.33) population of the Al p_z orbital to full (1.0) occupancy occurs in the region between the two minima and at a longer internuclear distance as the number of He atoms in the node is increased. It is thus seen that spin-orbit mixing is more rapidly quenched as the number of He atoms forming the polygon (*i.e.*, as the number of He atoms surrounding the Al on its nodal plane) increases. The He-He distance corresponding to the peak of the low-temperature pair correlation of liquid helium (3.5 Å)[36] provides

the upper limit for the He-He distances of the He atoms which make up the Al-centered polygons[37]. The Al-He distance of 4.2 Å corresponds both to the AlHe $1^2\Pi$ equilibrium internuclear distance and to the position of the $AlHe_n$ ground state minimum for $n > 4$ (cf. Figure 9). At this AlHe distance, a ring of 7(8) He atoms is found to have a He-He spacing of 3.6(3.2) Å. Thus a polygon containing 7 He atoms exhibits He-He distances which are too large. Therefore we conclude that at least 8 He atoms will collect around the Al atom. This has been shown above to be sufficient to quench the spin-orbit coupling.

2.4 Theory of intermolecular forces and its application to light-metal atom complexes.

The Hartree-Fock plus Dispersion method has two components: the uncorrelated energy, calculated at the Hartree-Fock self-consistent level, and the correlated energy, calculated by an inverse distance multipole expansion. Each term in the expansion is individually damped to account for charge-overlap.[22] These damping functions are modeled on the hydrogen triplet dimer, which can be calculated exactly. The size of the atoms is used to scale the amount of overlap by taking the inverse ratio of the ionization potential with hydrogen and raising it to 0.66 (so $\rho=(IP^H/IP^X)^{0.66}$), where ρ is the dimensionless distance scaling parameter and X is the atom or molecule of interest). This method does not include coupling between the exchange and correlation energies.

For the rare gas atoms, the HFD method has produced good potentials for the dimers[23] (errors in binding energy and equilibrium distance of 1% or less). Yet it is well-known that this method fails when "softer" atoms (with a low IP, i.e., alkalis) are involved. Because of the importance of "soft" atoms to the HEDM program we have studied how to improve the predictive ability of the HFD method for these atoms and their mixtures.

2.4.1 Dimers of Soft Atoms

For the alkali triplet dimers, the HFD error is large (30% or more) and increases down the group, always yielding too attractive potentials. The alkaline earth dimers are also calculated to be too attractive. The valence shells of these dimers have significantly more overlap than the corresponding hydrogen case. The extra attraction is a result of the HFD method treating them like undistorted spheres centered on each nucleus.

These are "soft" atoms, however, with easily distortable electron clouds. As the nuclei get closer together, the electrons resist overlapping and are moved off-center. Effectively, the nuclei continue to approach each other, while the electron clouds remain farther apart. So, in the standard HFD method, the multipole expansion is calculated at a distance that is too short, producing too attractive results.

As the electron clouds are pushed away from their respective nuclei, a quadrupole develops. Using the quadrupole moment calculated in Gaussian 98[31] and, treating the system as four point charges, we can determine the distance between the nuclei and the centers of the electron clouds. The alkali triplet dimers and Mg_2 show a "lag" of the internuclear distance of about 0.5 bohr. We refer to this additional term as the quadrupole correction, and the new method for calculating potentials as HFDQ. This is a first step towards including exchange-correlation coupling terms.

Using the new HFDQ method we have greatly reduced the error in the alkali triplet (and magnesium) dimer potential curves to 15% or less (in the well depth; to 1% for the distance). The remaining discrepancy is probably due to the shape of the distorted electron clouds; HFDQ still treats the clouds as spheres. The method works as well for mixtures of alkalis, for instance for the NaLi triplet (see table 8). When applied to alkali oligomers (e.g., trimers and tetramers) the errors decrease to about 10% (see table 9).

		ε/cm^{-1}	$R_m/Å$
Li_2	lit.	333.4	4.19
	HFDQ	331.318	4.175
	HFD	461.5	3.88
Na_2	lit.	174.96	5.09
	HFDQ	199.84	5.01
	HFD	250.3	4.7
K_2	lit.	254.1	5.77
	HFDQ	269.489	5.74
	HFD	445.92	5.24
Mg_2	lit.	429.6	3.89
	HFDQ	504.001	3.95
	HFD	702.65	3.66
NaLi	lit.	215.9	4.76
	HFDQ	252.974	4.61
	HFD	337.06	4.28

Table 8. Alkali triplet dimer potential well parameters from the HFD and HFDQ methods, compared to literature values.

The concept of distorted electron clouds also accounts for the non-additivity of the SCF repulsion Which turns out to be responsible for more than 90% of the additivity of the whole Na_3 potential (see the end of Section 2.1.2 and ref. 12). The HF energy of the trimer and tetramer show less repulsion than adding the SCF of the dimer pairs. With the softer atoms, the nuclei are able to approach closer because the electrons are pushed out of the way.

2.4.2 Mixtures of Soft and Hard Atoms

Neither HFD nor HFDQ work for mixtures of soft and hard atoms (e.g., the alkali-rare gas dimers). Most of the potentials have wells too shallow, but a few are just right, or even too deep. Why does the method fail? Could it be the difference in sizes of the atoms? Not likely, since LiH is too deep, while NaH is too shallow; LiHe is correct, while NaHe is again too shallow. And both alkali complexes with neon are much too shallow (see table 10).

Probably size is important, but only through the distortion of the electron cloud. As the hard partner approaches, the soft atom distorts around it, almost forming a dimple in which the hard atom sits. The distortion then slightly polarizes the hard partner allowing for increased correlation energies and greater attraction. Judging by the worse results obtained with HFDQ it is clear the shape of the distortion, and not just the distance, is important.

Further efforts at determining the shape of the electron cloud will improve our understanding of the alkali-alkali interaction, the alkali-noble gas mixtures and, ultimately, of the alkali-hydrogen interactions.

	Dimer		Trimer		Tetramer	
	ε/cm^{-1}	$R_m/Å$	ε/cm^{-1}	$R_m/Å$	ε/cm^{-1}	$R_m/Å$
Na lit.	175.0	5.09	835.8	4.40	3250	3.9
HFDQ	199.8	5.01	962.4	4.36	3566	3.83
HFD	250.3	4.7	1410	4.02	5200	3.64
Mg lit.	429.6	3.89	2630	3.37	8600	3.1
HFDQ	504.0	3.95	2200	3.55	8100	3.15
HFD	702.6	3.66	4050	3.22	14140	2.95

Table 9. Comparisons of potential well parameters for oligomers of Na and Mg.

LiH	ε/cm^{-1}	$R_m/Å$	**NaH**	ε/cm^{-1}	$R_m/Å$
lit.	4.24	6.12	lit.	4.11	6.35
HFDQ	4.87	5.99	HFDQ	3.95	6.32
HFD	4.89	5.98	HFD	3.91	6.34
LiHe			**NaHe**		
lit.	1.62	6.07	lit.	1.54	6.27
HFDQ	1.50	6.12	HFDQ	1.18	6.54
HFD	1.51	6.13	HFD	1.18	6.52
LiNe			**NaNe**		
lit.	8.78	5.12	lit.	8.0	5.3
HFDQ	5.84	5.4	HFDQ	4.64	5.70
HFD	6.00	5.36	HFD	4.68	5.68
LiAr			**NaAr**		
lit.	42.2	4.89	lit.	41.7	5.01
HFDQ	34.7	5.02	HFDQ	34.8	5.05
HFD	42.4	4.72	HFD	37.8	4.86
LiKr			**NaKr**		
lit.	68.0	4.78	lit.	68.9	4.74
HFDQ	45.3	5.12	HFDQ	44.8	5.22
HFD	57.8	4.74	HFD	53.7	4.85

Table 10. Comparisons of potential well paramters for several soft/hard atom combinations.

2.5 Progress towards assembling a facility for stimulated Raman spectroscopy (SRS) in doped and undoped hydrogen clusters.

2.5.1 The SRS experiment

In recent years, the experimental feasibility of observing a superfluid phase of *para*-hydrogen (p-H_2) has been investigated in various contexts;[38,39,40,41,42] to date, the existence of such a phase has not been conclusively proven.

The goal of an ongoing effort here at Princeton is to produce ultracold p-H_2 droplets of a few hundred to a few thousand molecules in a supersonic expansion,[43] which will be spectroscopically investigated using SRS. Such droplets have good prospects for being superfluid because both their small size and their very short lifetime in the experiment decrease the chance of freezing nucleation: it may then be possible for them to be supercooled so much below the triple point of p-H_2 that Bose-Einstein condensation occurs.

Spectroscopic evaluation of the possibly superfluid aggregation state of the hydrogen nanodroplets calls for Raman scattering, since infrared transitions in condensed molecular hydrogen are very weak, induced only by lattice defects, surfaces, and impurities. Due to the low number density of hydrogen molecules in a cluster beam, *stimulated* Raman scattering is called for because of its increased efficiency. During stimulated Raman scattering, a high-energy photon (738 nm in our case) is absorbed while at the same time emission of a lower-energy photon (1064 nm) is stimulated. The difference in energy promotes a hydrogen molecule to the v=1 vibrationally excited state. Subsequent relaxation back to the ground state leads to partial evaporation of the hydrogen nanodroplet. As in the IR spectroscopy of doped ^{4}He droplets,[44] the decrease in beam flux can be detected with a cold bolometer.

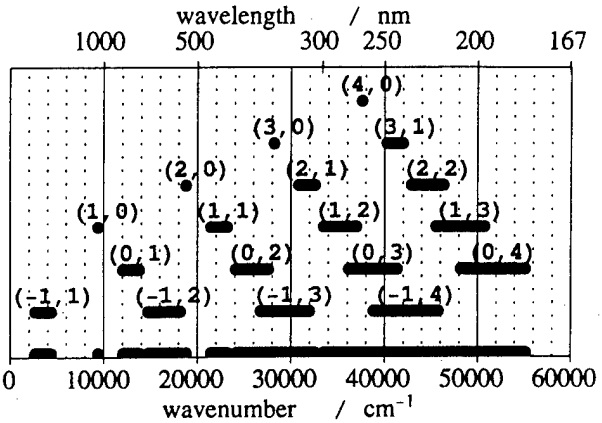

Figure 10. Spectral regions accessible with the Indigo Ti:Al_2O_3 in combination with the Antares Nd:YAG. The label (m,n) refers to mixing the m^{th} harmonic of the Nd:YAG with the n^{th} harmonic of the Ti:Al_2O_3. For example, (-1,3) is the difference frequency between the tripled Ti:Al_2O_3 and the fundamental of the Nd:YAG. The bottom line summarizes the accessible wavelength ranges.

2.5.2 The laser setup

The laser system for stimulated Raman scattering in hydrogen consists of a continuously tunable Ti:Al_2O_3 "Indigo" laser that produces narrow band radiation around 738nm, and a Q-switched, cavity-dumped Nd:YAG laser "Antares" operating at 1064nm. The short pulses produced by the Indigo can easily be frequency doubled and tripled; when combined with the Antares and its harmonics, a very large range of frequencies can be covered, in which a wealth of high-resolution experiments can be performed (see Figure 10).

2.5.3 The Indigo Ti:Al_2O_3 cavity

The narrow-band output of the Indigo is produced in a modified Fox-Smith resonator[45] consisting of a high reflector (HR), an output coupler (OC), a grating, and a tuning mirror (see Figure 11). There are two interfering light paths in such a resonator: between the HR and the OC via specular reflection off the grating (path A), and between the HR and the tuning mirror via first-order diffraction off the grating (path B). The latter path is wavelength selective, because the combination of grating and tuning mirror only reflects rays of a very narrow wavelength range back onto themselves.

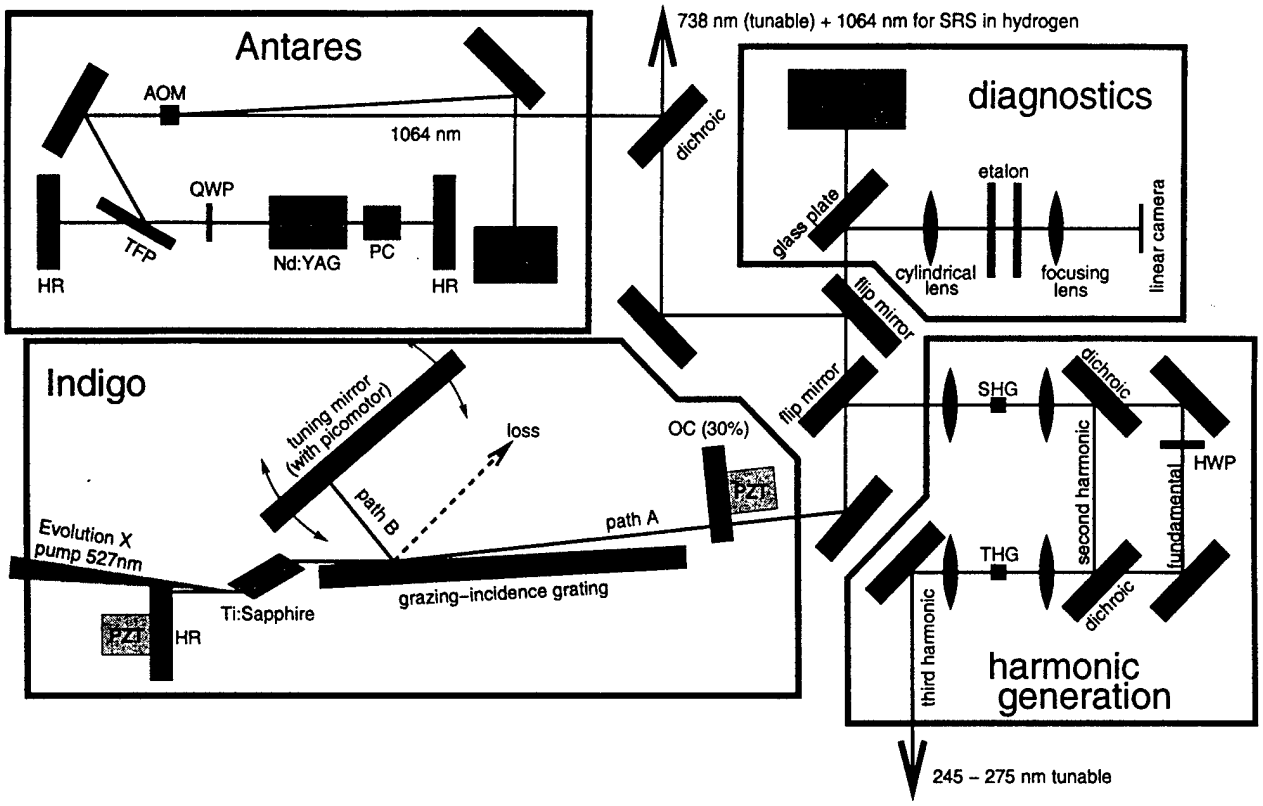

Figure 11. Setup of the laser system. The Indigo is a tunable, pulsed single-mode Ti:Al_2O_3 laser that can be frequency-doubled and -tripled. The Antares is a pulsed Nd:YAG laser synchronized with the Indigo, to be used for stimulated Raman scattering or frequency mixing with the Indigo. The diagnostics are used both for wavelength measurements and mode stabilization of the Indigo.

The lasing threshold of the Indigo resonator is greatly reduced if we have constructive interference between the two light paths. If all other cavity elements are fixed, we can change the length of path A by displacing the OC, which is done by applying a voltage to the OC PZT. This shifts the absolute wavelengths at which constructive interference occurs, and we can thus make sure that at the maximum of the wavelength selectivity of path B we simultaneously have constructive interference of the two light paths.

Furthermore, we must place the HR at a position where both light paths simultaneously have a node, so that the two light paths actually form an eigenmode of the laser cavity. We do this by applying a voltage to the HR PZT. This is a modification to the original design of the Indigo by Positive Light, Inc., in which there was no provision for such fine-tuning. We have found, however, that single-mode operation of the Indigo cannot be achieved without this additional degree of freedom.

We have put in place a computer-based feedback system that observes the spectral quality of each laser shot of the Indigo through a plane-parallel étalon (FSR 4.4 GHz) imaged with a linear camera, and then adjusts the voltages on the two cavity PZTs accordingly. Misplacement of the HR is detected by observing the emergence of neighboring cavity modes, spaced by about 800 MHz from the main laser output frequency. Misplacement of the OC is detected by the emergence of neighboring maxima of constructive interference, spaced by about 3 GHz from the main laser frequency. The different spacings of cavity modes and interference maxima easily allow their identification in the feedback algorithm. With this system in place, single-mode operation of the Indigo can usually be established within a few hundred milliseconds. As the tuning mirror is rotated slowly and thus the wavelength selected by path B is scanned,

the positions of the HR and OC mirrors are adjusted continuously, allowing smooth tuning of the single-mode output of the Indigo. The linear tunability is now only limited by the gain medium.

After stabilization, the Indigo puts out single-mode radiation that is essentially transfer limited by the pulse duration of approximately 10 ns. Pumped by a 10 W "Evolution X" diode-pumped, intra-cavity frequency-doubled Nd:YLF laser, the Indigo can deliver up to 1.5 mJ pulses around 800 nm at 1 kHz repetition rate.

The wavelength of the Indigo radiation is monitored with a Burleigh WA-4500 wavemeter. For absolute calibration, we have furthermore measured the two-photon absorption spectrum of rubidium vapor around 778.1 nm (see Figure 12). Combined, these measurements determine the Indigo frequency to within less than 100 MHz.

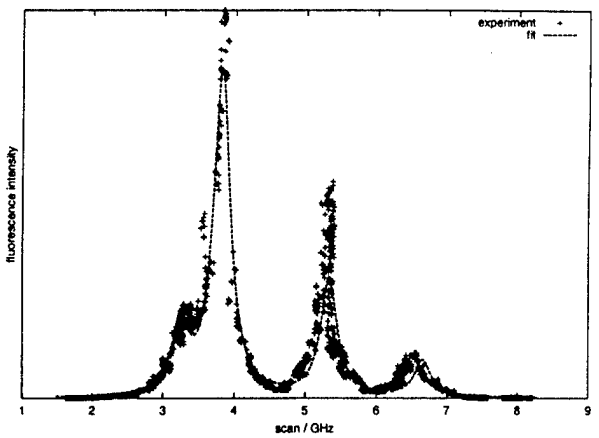

Figure 12. The two-photon fluorescence spectrum of gas-phase rubidium, as measured with the Indigo. The main peak corresponds to the $5S_{1/2}$ (F=3) $\rightarrow$ $5D_{5/2}$ (F=5) transition in ^{85}Rb, and is at 385 285 142 378.280 $\pm$ 2 kHz.[46]

2.5.4 Indigo Harmonics Generation

The high peak power of the Indigo invites generation of second- and third-harmonic laser radiation. Second-harmonic generation (SHG) is done by focusing the fundamental into an angle-tuned LBO crystal, and produces up to 200 μJ pulses around 400 nm. Third-harmonic radiation is produced (THG) by co-focusing the fundamental and the second harmonic into an angle-tuned BBO crystal. Since the polarization of the secondharmonic is orthogonal to the fundamental due to birefringence phase matching in the LBO crystal, we rotate the plane of polarization of the fundamental by 90° with a half-wave plate (HWP) after separating it from the second harmonic with a dichroic mirror. We can produce up to 3.5 μJ of UV light at 260 nm in pulses of about 7 ns length.

We expect to receive the components for fourth-harmonic generation (FHG) soon. This will allow us to extend the range of accessible wavelengths all the way down to the limit of vacuum UV.

The angles of all the harmonic-generation crystals can be adjusted by picomotor screws, which allow software control of the phase matching condition as the Indigo is scanned in frequency.

2.5.5 Antares Nd:YAG Cavity

We have converted a Coherent Antares cw Nd:YAG laser to pulsed operation, in which it can produce 10 ns pulses at a repetition rate of up to 3 kHz, and with a pulse energy of up to 2 mJ (measured at 1 kHz). This was achieved by inserting into the cavity a KD*P Pockels cell (PC), a quarter-wave plate (QWP), and a thin film polarizer (TFP), in the setup schematized in Figure 10. Switching the Pockels cell on starts the buildup of laser radiation in the cavity, and switching it off dumps the entire laser power out of the cavity within about one round-trip time. This "dumped" pulse can be synchronized with the Indigo pulse to within less than 2 ns, which is sufficient for stimulated Raman scattering experiments.

The unseeded Q-switched Antares has a spectral width of about 0.6 cm^{-1}, which is unacceptable for high-resolution Raman spectroscopy. To remedy this, we have added a Lightwave S-100 seed laser that reduces the line width of the Antares to single- or double-mode operation. A circuit for locking the Antares cavity length to the seeder wavelength, to produce single-mode output, remains to be

implemented. However, the cavity modes of the Antares are spaced by only 140 MHz, and therefore operation on two modes introduces a frequency uncertainty comparable to the Indigo line width, and further narrowing may turn out to be unnecessary.

3.0 References

[1] J. Reho, C. Callegari, J.Higgins, K.K. Lehmann, and G.Scoles. *Farad. Discuss.* **108**, 161 (1997).

2 F. Stienkemeier, J. Higgins, C. Callegari, W.E. Ernst, S.I. Kanorsky, and G. Scoles. *Z. für Physik D.* **38**, 253 (1996).

[3] J. Pascale, *Technical Report, Service de Physique des Atoms et des Surfaces* C.E.N.Saclay, Gif sur Yvette-Cdex, France (1983).

[4] J.L. Persson, Q. Hui, Z.J. Jakubek, M. Nakamura, and M. Takami. *Phys Rev. Lett.* **76**, 1501 (1996).

[5] A. Derevianko, *private communication.*

[6] J. Reho, J. Higgins, C. Callegari, K.K. Lehmann, G. Scoles. *J. Chem. Phys.* **113**, 9686 (2000).

[7] J. Reho, J. Higgins, K.K. Lehmann, and G. Scoles. *J. Chem. Phys.* **113**, 9694 (2000).

[8] J.Higgins, W.E. Ernst, C. Callegari, J. Reho, K.K. Lehmann, and G. Scoles. *Science* **273**, 629 (1996).

[9] J.Higgins, W.E. Ernst, C. Callegari, J. Reho, K.K. Lehmann, and G. Scoles. *Phys. Rev. Lett.* **77**, 4532 (1996).

[10] For the lifetime of atomic Na (3P), see E.B. Saloman. *Spectrochimica Acta* **48B**, 1139 (1993). For the lifetime of the $(B)^1\Pi_u$ state, see W. Demtröder, W. Stetzenbach, M. Stock, and J. Witt. *J. Mol. Spec.* **61**, 382 (1976).

[11] J.H. Reho, J.H.P. Higgins, M. Nooijen, K.K. Lehmann, G. Scoles, and M. Gutowski. *J. Chem. Phys.* **115**, 10265 (2001).

[12] J. Higgins, T. Hollebeek, J. Reho, T.S. Ho, K.K. Lehmann, G. Scoles, and M. Gutowski. *J. Chem. Phys.* **112**, 5751 (2000).

[13] J.H. Reho, J.P. Higgins, and K.K. Lehmann. *Farad. Discuss.* **118**, 33 (2001).

[14] T. Kinoshita, K. Fukuda, and T. Yabuzaki. *Phys. Rev. B*, **54**, 6600.

[15] J. Reho, U. Merker, M.R. Radcliff, K.K. Lehmann, and G. Scoles, *J. Phys. Chem. A*, **104**, 3620 (2000).

[16] Y. Moriwaki and N. Morita. *Eur. Phys. J. D.* **5**, 53 (1999).

[17] F. Stienkemeier, F. Meier, H. O. Lutz, *J. Chem. Phys.* **107**, 10816 (1997).

[18] Q. Hui, Ph.D. thesis, Graduate School of Science and Engineering, Saitama University (1997).

[19] A. Lurio. *Phys. Rev.* **136**, 376 (1964).

[20] J. Reho, U. Merker, M.R. Radcliff, K.K. Lehmann, and G. Scoles, *J. Chem. Phys.* **112**, 8409 (2000).

[21] F. Ancilotto, P. B. Lerner, and M. W. Cole, *J. Low Temp. Phys.* **101**, 1123 (1995).

[22] C. Douketis, G. Scoles, S. Marchetti, M. Zen, and A. Thakkar. *J. Chem. Phys.* **76**, 3057 (1982).

[23] M.R. Radcliff, K.K. Lehmann, and G. Scoles, *to be published.*

[24] E. Czuchaj, H. Stoll, and H. Preuss, *J. Phys. B*, **20**, 1487 (1987).

[25] U. Kleinekthofer, private communication.

[26] K. Szalewicz and G. Murdachaew, *private commun.*

[27] H. Partridge, J.R. Stallcop, and E. Levin. *J. Chem. Phys.* **115**, 6471 (2001).

[28] J. Dupont-Roc, M. Himbert, N. Parloff, and J. Treiner. *J. Low Temp. Phys.* **81**, 31 (1990).

[29] F. Dalfovo. *Z. Phys. D* **29**, 61 (1994).

[30] M. Casas, F. Dalfovo, A. Lastri, Ll. Serra, and S. Stringari. *Z. Phys. D* **35**, 67 (1995).

[31] Calculated from Einstein coefficients given in: *Handbook of Chemistry and Physics, 79th edition*, edited by D.R. Lide, CRC Press, Boca Raton (1998).

[32] *Gaussian 98 (Revision A.7)*, M.J. Frisch, G.W. Trucks, H.B. Schlegel, G.E. Scuseria, M.A. Robb, J.R. Cheeseman, V.G. Zakrzewski, J.A. Montgomery, Jr., R.E. Stratmann, J.C. Burant, S. Dapprich, J.M. Millam, A.D. Daniels, K.N. Kudin, M.C. Strain, O. Farkas, J. Tomasi, V. Barone, M. Cossi, R. Cammi, B. Mennucci, C. Pomelli, C. Adamo, S. Clifford, J. Ochterski, G.A. Petersson, P.Y. Ayala, Q. Cui, K. Morokuma, D.K. Malick, A.D. Rabuck, K. Raghavachari, J.B. Foresman, J. Cioslowski, J.V. Ortiz, A.G. Baboul, B.B. Stefanov, G. Liu, A. Liashenko, P. Piskorz, I. Komaromi, R. Gomperts, R.L. Martin, D.J. Fox, T. Keith, M. A. Al-Laham, C.Y. Peng, A. Nanayakkara, C. Gonzalez, M. Challacombe, P.M. W. Gill, B.G. Johnson, W. Chen, M.W. Wong, J.L. Andres, M. Head-Gordon, E.S. Replogle and J.A. Pople, Gaussian, Inc., Pittsburgh PA, 1998.

[33] S.D. LePicard, B. Bussery-Honvalult, C. Rebrion-Rowe, P. Honvault, A. Canosa, J.M. Launay, and B.R. Rowe. *J. Chem. Phys.* **1998**, *108*, 10319.

[34] J.M. Standard and P.R. Certain. *J. Chem. Phys.* **83**, 3002 (1985).

[35] H.L. Kramer, D.R. Herschbach. *J. Chem. Phys.* **1970**, *53*, 2792.

[36] H.N. Robkoff, R.B. Hallock. *Phys. Rev. B.* **1981**, *25*, 1572.

[37] For a He droplet the size of those employed in our experiments, the density in the region of the center is expected to approach that of the bulk liquid, so that the He-He distance could be gotten from the peak of the pair correlation known from bulk liquid helium as is done in the text. However, the inclusion of the dopant increases the local density around the cavity in which the solute atom resides, and thus the He-He distance of the He_n polygons would be expected to be *smaller* than is found from consideration of the bulk liquid.

[38] M. Schindler, A. Dertinger, Y. Kondo, and F. Pobell, Phys. Rev. B **53**, 11451 (1996).
[39] F. C. Liu, Y. M. Liu, and O. E. Vilches, Phys. Rev. B **51**, 2848 (1995).
[40] M. C. Gordillo and D. M. Ceperley, Phys. Rev. Lett. **79**, 3010 (1997).
[41] P. Sindzingre, D. M. Ceperley, and M. L. Klein, Phys. Rev. Lett. **67**, 1871 (1991).
[42] S. Grebenev, M. Hartmann, M. Havenith, B. Sartakov, J. P. Toennies, and A. F. Vilesov, J. Chem. Phys. **112**, 4485 (2000).
[43] M. Kappes and S. Leutwyler, in *Atomic and molecular beam methods*, edited by G. Scoles (Oxford University Press, New York, 1988), Vol. 1, p. 380.
[44] C. Callegari, R. Schmied, K. K. Lehmann, and G. Scoles, J. Chem. Phys. **115**, 10090 (2001).
[45] D. J. Binks, L. A. W. Gloster, T. A. King, and I. T. McKinnie, Applied Optics **36**, 9371 (1997).
[46] D. Touahri, O. Acef, A. Clairon, J. J. Zondy, R. Felder, L. Hilico, B. deBeauvoir, F. Biraben, and F. Nez, Optics Communications **133**, 471 (1997).

4.0 Publications resulting from AFOSR Grant #F49620-98-1-0045

1) **Spin-orbit effects in the formation of the Na-He excimer on the surface of He clusters.** J. Reho, C. Callegari, J. Higgins, W.E. Ernst, K.K. Lehmann, and G. Scoles. *Farad. Discuss.* **108**, 161-174 (1997).

2) **Beam Depletion Spectroscopy of Alkali Atoms (Li, Na, K) Attached to Highly Quantum Clusters.** C. Callegari, J. Higgins, F. Stienkemeier and G. Scoles. *J. Phys.Chem. A* 102 (1), 95-101 (1998).

3) **He cluster-isolation spectroscopy: alkali dimers in the triplet manifold.** J. Higgins, J. Reho, C. Callegari, W. E. Ernst, F. Stienkemeier and G. Scoles. *J. Phys. Chem. A* 102 (26), 4952-4965 (1998).

4) **Helium cluster isolation spectroscopy**. J.P. Higgins, Ph.D. thesis, Princeton University, Department of Chemistry. (1998).

5) **Potential of an ionic impurity in a large ^{4}He cluster.** K.K. Lehmann and J. Northby, *Molecular Physics,* 97 (5), 639-644 (1999).

6) **Potential of an neutral impurity in a large ^{4}He cluster,** K.K. Lehmann, *Molecular Physics,* 97 (5), 645-666 (1999).

7) **Spectroscopy and dynamics of Al atoms solvated in superfluid helium nanodroplets.** J.H. Reho, U. Merker, M. R. Radcliff, K. K. Lehmann, and G. Scoles. *J. Phys. Chem. A* 104 (16), 3620-3626 (2000).

8) **On the nature of bonding in small Mg clusters.** J. M. Sin, S. Nayak, and G.Scoles in Cluster and Nanostructure Interfaces, P. Jena Ed., World Scientific, 2000, page 345.

9) **On the importance of exchange effects in three-body interactions: The lowest quartet state of Na_3.** J. Higgins, T. Hollebeek, J. Reho, T. S. Ho, K. K. Lehmann, H. Rabitz, G. Scoles and M. Gutowski. *J. Chem. Phys.* 112 (13), 5751-5761, (2000).

10) **Reproducing kernel technique for extracting accurate potentials from spectral data: Potential curves of the two lowest states $X^1\Sigma_g^+$ and $a^3\Sigma_u^+$ of the sodium dimer.** T.-S. Ho, H. Rabitz, and G. Scoles. *J. Chem. Phys.* 112, (14), 6218-6227 (2000).

11) **Spectroscopy of Mg atoms solvated in helium nanodroplets.** J. Reho, U. Merker, M.R. Radcliff, K. K. Lehmann, and G. Scoles. *J. Chem. Phys.* 112 (19), 8409-8416 (2000).

12) **Alkali-helium exciplex formation on the surface of helium nano-droplets. I. Dispersed emission spectroscopy.** J. Reho, J. Higgins, C. Callegari, K. K. Lehmann, and G. Scoles. *J. Chem. Phys.*, 113, (21) 9686-9693 (2000).

13) **Buoyancy Corrections for the Potential of an Impurity in a ^{4}He nanodroplet,** K.K. Lehmann, *Molecular Physics,* 98 (23), 1991-1993 (2000).

14) **Alkali-helium exciplex formation on the surface of helium nanodroplets. II. A time-resolved study.** J. Reho, J. Higgins, K. K. Lehmann, and G. Scoles. *J. Chem. Phys.* 113 (21), 9694-9701 (2000).

15) **Time-resolved apectroscopy of atoms and molecular dopants in and on Helium nanodroplets.** J.H. Reho, Ph.D. thesis, Princeton University, Department of Chemistry. (2000).

16) **Spectroscopy in, on and off a beam of superfluid helium nanodroplets.** J. Higgins, J. Reho, F. Stienkemeier, W. E. Ernst, K. K. Lehmann, and G. Scoles. Atomic and Molecular Beams: The State of the Art 2000, Part VI, p.723-754. R. Campargue Ed., Springer-Verlag (2000).

17) **Photoinduced nonadiabatic dynamics in quartet Na_3 and K_3 formed using helium nanodroplet isolation.** J. H. Reho, J. H. P. Higgins, M. Nooijen, K.K. Lehmann, G. Scoles, and M. Gutowski. *J. Chem. Phys.* 115, (22) 10265-10274 (2001).

18) **Dynamics of the $1^3\Pi_g$ State of K_2 on Helium Nanodroplets.** J. H. Reho, J. P. Higgins, and K. K. Lehmann, *Royal Society of Chemistry, Faraday Discussions* (Cluster Dynamics) 118, 33-42 (2001).

19) **Faraday Discussions, General Discussions,** *Royal Society of Chemistry,* K. K. Lehmann, 118, 43-63 (2001).

5.0 Interactions

5.1 Invited papers given by G. Scoles at National and International Meetings in which the work carried out under the present grant was discussed (Total = 20)

98.1 *Probing barriers to the aggregation of light metal atoms using He cluster isolation spectroscopy.* HEDM Contractors Meeting, Monterey, CA., May 20-22, 1998.

98.2 *Recent results of helium cluster isolation spectroscopy.* ACS Nat.Meet.in Boston, MA., August 23-28, 1998.

98.3 *Spectroscopy and dynamics in liquid helium clusters.* European Meeting of the Mol.Beams Group of the Royal Soc.of Chemistry. Lunteren, NL, Sept. 2-4, 1998.

98.4 *Chemical dynamics in liquid helium clusters.* Chem.Dyn.Symp. in honor of Prof.G. G. Volpi, Perugia, Italy, July 10-13, 1998.

98.5 *Photoassociation reactions in liquid helium clusters.* Workshop on Spectroscopy in Liq. He Clusters (DFG). Bad Honnef, DBR, Oct. 30-31, 1998.

98.6 *The photons that came in from the cold: high resolution spectroscopy in liquid helium clusters.* Annual Meeting of the High Res.Spectroscopy Group of the Royal Soc. of Chem., Nottingham, UK, Dec. 20-22, 1998.

99.1 *Recent results in He cluster-isolation spectroscopy.* Symposium on Interfacial Dynamics, Lincei Academy, Rome, Italy, March 25-26, 1999.

99.2 *The solvation of light metal atoms in liquid He droplets.* AFOSR-HEDM Meeting, Cocoa Beach, FL., June 7-11, 1999.

99.3 *Molecule formation and molecular spectroscopy in and on liquid He clusters.* Trapping, pectrocopy and Collisions of Ultracold Molecules. ITAMP Workshop, Boston, MA, July 1-3, 1999.

99.4 *How simple are superfluid He clusters?* Gordon Conference on Simple Systems, Newport,R.I., July 11-15, 1999.

99.5 *Desorption Induced by Electronic Transitons of Alkali Metal Atoms and Oligomers from the Surface of Superfluid Liquid Helium Droplets.* DIET-8, S. Alfonso, Long Branch, N.J., Sept.27-Oct. 2, 1999.

00.1 *Superfluid Helium Nanodroplets are Cool Spectrographic Matrices.* Symposium 2000, University of Guelph, Waterloo, Canada, June 2, 2000.

00.2 *Spectroscopy of Metal Atoms in and on Liquid Helium Nanodroplets.* IV. Workshop On Quantum Fluid Clusters, Ringberg Schloss, Kreuth-Oberhof, Bavaria, June 25-28, 2000.

00.3 *Liquid helium clusters as cool nanomatrices for infrared spectroscopy.* ISSPIC 10, Atlanta, GA., October 11-15, 2000.

00.4 *Solubility of metal atoms in quantum clusters and stability of small H_2 clusters containing a Group III atom.* 2000 Air Force High Energy Density Matter (HEDM) Contractors Conference, Park City, Utah, October 24-26, 2000.

01.1 *Unusual physical and chemical processes in superfluid He nanodroplets.* Second S. Lundquist Conference on the Advancing Frontiers of Condensed Matter Physics, Trieste, July 6, 2001.

01.2 *He nanodroplet isolation spectroscopy.* 2001 Int. Conference on Matrix Spectroscopy. S. Poreba (Poland) July 9, 2001.

01.3 *Overview of what we learn from clusters on 3-body forces.* 2001 ACS Meeting, Chicago, IL., July 26, 2001 (Chair remarks).

01.4 *Helium nanodroplet isolation spectroscopy.* XVII Colloquium on High Res. Spectroscopy. Papendal (The Netherlands) Sept. 9, 2001.

01.5 *Far-from-equilibrium chemistry in superfluid heliun nanodroplets.* XXVIII Biannual Meeting of the Royal Spanish Physical Society (Plenary Talk) Sevilla, Sept.25, 2001.

5.2 Invited papers given by K. K. Lehmann at National and International Meetings in which work carried out under the present grant was discussed. (Total = 17)

98.1 The 1998 Gordon Research Conference on Molecular and Ionic Clusters, Ventura, CA,, Jan.4-9, 1998.

98.2 The 1998 Gordon Research Conference on Atomic and Molecular Interactions, New London, N.H., June 28-July 3, 1998.

98.3 The American Society Meeting, Boston, MA., Aug. 23-27, 1998.

99.1 CCP6 Conference on Ro-vibrational Spectroscopy, Aberdeen , Scotland, April 11-14, 1999.

99.2 Gordon Research Conference on the Chemistry and Physics of Matrix Isolate Species, JULY 11, 16, 1999.

99.3 Inspired by Herzberg: Spectroscopy for the Year 2000, Cornwall, Ontario, Oct.30-Nov.3, 1999.

00.1 Workshop on Quantum liquids in confined geometries, university of Valencia, Spain, February 1-4, 2000.

00.2 Workshop on Quantum Fluid Clusters, Ringberg Schloss, Oberhof, Germany. June 25-28, 2000.

00.3 American Chemical Society Fall Meeting, Washington, D.C., August 20-25, 2000.

00.4 The 16^{th} International Conference on High Resolution Molecular Spectroscopy, Prague,Czech Republic, September 3-7, 2000.

00.5 2000 Research Meeting on Atomic, Molecular and Optical Physics, Maryland, September 27-29, 2000.

00.6 International Laser Sciences-XVI, Providence RI, October 22-26, 2000.

01.1 Sixth Conference on Molecular Dynamics, Laguna Beach, CA. Feb. 28-Mar. 3, 2001.

01.2 Farady Discussions 118: Cluster Dynamics, Durham, U.K., April 18-20, 2001.

01.3 APS Division of Atomic, Molecular, and Optical Physics Meeting, London, Ontario, May 16-18, 2001.

01.4 Air Force Office of Scientific Research Contractors Meeting, Irvine, CA., May 21-23, 2001

01.5 Fifty-sixth International Symposium on Molecular Spectroscopy, Columbus, OH., June 11-15, 2001.

5.3 Invited seminars given by G. Scoles in which work carried out under this grant was discussed. (Total = 24)

99.1 Phys. Dept., University of Delaware, Feb. 24

99.2 University of Florence, Italy, March 16

99.3 University of Bologna, Italy, March 1

99.4 University of Genova, Italy, March 3

99.5 Stevens Institute of Technology, Hoboken, N. J., Nov. 17

99.6 University of Wisconsin, Chemistry, Nov. 30

00.1 Phys. Dept. SISSA, Trieste (Italy) Jan. 11

00.2 Chem. Dept., Ohio State University, Feb. 23

00.3 Chem. Dept., Ohio State University, Feb. 25

00.4 Phys. Dept., Harvard, March 8

00.5 Phys. Dept., U.of Barcelona (Spain), April 26

00.6 Nat.Res.Council of Canada, Ottawa, May 12

00.7 Phys. Dept., U. of Genova (Italy), June 14

00.8 Chem.Dept. Tech. Univ of Munich (Germany), June 30

00.9 Chem.Dept., Utah State University, Oct. 23

01.1 ETH Zurich, Dept. of Chemistry, May 9

01.2 Dept. of Chem., Univ. of Geneva, May 15

01.3 Dept. of Phys.Chem., Univ. of Basel, May 16

01.4 Dept. of Phys. Chem., EPFL, Lausanne, May 17

01.5 Dept. of Phys. Chem., EPFL, Lausanne, May 18

01.6 Dept. of Phys.Chem., Univ. of Bern, May 22

01.7 Dept. Phys. Chem., Univ. of Helsinki, June 18

01.8 Dept. of Chem., Univ. of Alberta, Edmonton (Canada) Nov.21, 22

01.9 Dept. of Physics, Penn State Univ., College Park, PA, Dec. 7

5.4 Invited seminars given by Kevin Lehmann in which work carried out under this grant was discussed. (Total = 8)

97.1 Department of Chemistry, New York University, Dec. 19, 1997.

98.1 Department of Chemistry, Georgia Technical University, Atlanta, GA., Oct. 29, 1998.

98.2 Department of Chemistry, Emory University, Atlanta, GA., Oct.30, 1998.

98.3 Department of Physics, University of Rhode Island, Dec. 11, 1998.

99.1 George Harrison Spectroscopy Laboratory, MIT, Oct. 19, 1999.

01.1 Department of Chemistry, Harvard University, Feb. 15, 2001.

01.2 Department of Chemistry, University of Southern California, Feb. 26, 2001.

01.3 Department of Chemistry, University of Wisconsin at Eau Claire, Oct. 19, 2001

5.5 Contributed papers at national and international meetings by other members of the group (Total = 12)

J. Higgins: *Helium Cluster Isolation Spectroscopy of Alkali Dimers in the Triplet Manifold.* Gordon Conference on Molecular and Ionic Clusters. Ventura, CA. Jan. 4-9, 1998. (poster presentation)

J. Reho: *Time-resolved Spectroscopy of* Na *Atoms and Oligomers on the Surface of* He *Clusters.* The 13th Symposium on Chemical Physics, Waterloo, ON, Canada. Oct. 24-26, 1997 (poster presentation)

J. Reho: *Non-adiabatic Processes in the Photodissociation of Quartet State* Na_3 *and* K_3. 53rd Ohio State University International Symposium on Molecular Spectroscopy. Columbus, OH. June 15-19, 1998. (oral presentation)

J. Reho: *Direct State-selective Measurement of Cooling Rates of Vibrationally Excited* $1^3\Pi_g^+$ Na_2 *on the Surface of Helium Clusters.* 53rd Ohio State University International Symposium on Molecular Spectroscopy. Columbus, OH. June 15-19, 1998. (oral presentation)

J. Reho: *Dynamics of Optically-excited Alkali Metal Dimers and Trimers on the Surface of Helium Clusters.* 216th ACS National Meeting. Boston, MA. Aug. 23-27, 1998. (oral presentation)

M. Radcliff: *Charge Distribution Deformation in van der Waals Complexes Involving Atoms With Low Ionization Potentials.* 17th Symposium on Chemical Physics, Waterloo, ON, Canada. Nov. 9-11, 2001. (oral presentation)

M. Radcliff: *Charge Distribution Deformation in van der Waals Complexes Involving Atoms With Low Ionization Potentials.* 2nd PUUDel Workshop on Intermolecular Interactions, Newark, DE. Oct. 12, 2001. (oral presentation)

M. Radcliff: *Spectroscopy of* Mg *Atom-Doped Helium Nanodroplets.* 55th Ohio State University International Symposium on Molecular Spectroscopy. Columbus, OH. June 12-16, 2000. (oral presentation)

M. Radcliff: *Spectroscopy of* Al *Atoms Solvated in Helium Nanodroplets.* 55th Ohio State University International Symposium on Molecular Spectroscopy. Columbus, OH. June 12-16, 2000. (oral presentation)

M. Radcliff: *Spectroscopy of Atoms in Helium Nanodroplets.* 1st PUUDel Workshop on Intermolecular Interactions, Princeton, NJ. June 15, 2000. (oral presentation)

M. Radcliff: *Studies of* Mg *Atoms Solvated in Helium Nanodroplets.* 15th Symposium on Chemical Physics, Waterloo, ON, Canada. Nov. 5-7, 1999. (poster presentation)

M. Radcliff: *Non-Adiabatic Processes in the Photodissociation of Quartet State Sodium Trimer.* 13th Symposium on Chemical Physics, Waterloo, ON, Canada. Oct. 24-26, 1997. (poster presentation)

6.0 Honors and Awards

During the period of tenure of this grant the PI has received the following honors and awards:

1997 - Elected Fellow of the Royal Society (UK)

1999 - Samuel McElvain Lecturer, University of Wisconsin, Madison

2000 - Honorary Science Doctorate from the University of Waterloo (Canada)

2000 - Elected Foreign Member of the Royal Academy of Arts and Sciences of The Netherlands

2000 - The 2000 Chemical Physics Symposium of the University of Waterloo (Canada) was dedicated to the P.I. 65th Birthday.

2001 Gunning Lecturer at the University of Alberta (Canada)

2002 Peter Debye Award for Physical Chemistry of the ACS